Superparamagnetic Twist-Type Actuators with Shape-Independent Magnetic Properties and Surface Functionalization for Advanced Biomedical Applications

Christian Peters, Olgaç Ergeneman, Pedro D. Wendel García, Michelle Müller, Salvador Pané,* Bradley J. Nelson, and Christofer Hierold*

Directed nanoparticle self-organization and two-photon polymerization are combined to enable three-dimensional soft-magnetic microactuators with complex shapes and shape-independent magnetic properties. Based on the proposed approach, single and double twist-type swimming microrobots with programmed magnetic anisotropy are demonstrated, and their swimming properties in DI-water are characterized. The fabricated devices are actuated using weak rotating magnetic fields and are capable of performing wobble-free corkscrew propulsion. Single twist-type actuators possess an increase in surface area in excess of 150% over helical actuators with similar feature size without compromising the forward velocity of over one body length per second. A generic and facile combination of glycine grafting and subsequent protein immobilization exploits the actuator's increased surface area, providing for a swimming microrobotic platform with enhanced load capacity desirable for future biomedical applications. Successful surface modification is confirmed by FITC fluorescence.

1. Introduction

Microrobotic devices are promising tools for various biomedical applications such as minimal invasive surgery, targeted drug delivery, remote sensing and single cell manipulation.[1,2] Swimming microrobots have performed tasks such as contact and non-contact micromanipulation as well as cargo transportation utilizing confinement.[3,4] Additional functionalities such as on-demand targeted drug delivery and remote sensing can be realized through the application of surface coatings and hyperthermia.[5–7] Surface coatings can inhibit unspecific protein absorption and increase blood circulation time,[8] enable fluorescence tracking in non-transparent environments,[3,9] as well as targeted drug delivery.[6,10] Hyperthermia may be applied to selectively attack target cells[11] or in combination with surface coatings for on-demand drug release.[12] From an actuation point of view, one of the most efficient transportation vehicles for these surface loads is the bio-inspired artificial bacterial flagella.[13] It adapts the helical tail of the *E. coli* bacteria and can be actuated wirelessly using weak rotating magnetic fields, mimicking the well-known cork-screw propulsion at the low Reynolds regime.[14] A variety of magnetic swimming microrobots has evolved based on this approach.[7] Recently, helical superparamagnetic swimming microrobots have been demonstrated.[15–17] These swimming microrobots are soft-magnetic in nature and exhibit geometry-dependent magnetic properties. The shape anisotropy limits both the geometrical freedom with respect to device design as well as efficient device actuation.[15] Kim et al. proposed the alignment of superparamagnetic nanoparticles while cross-linking a liquid polymer composite in order to establish a shape-independent anisotropy, referred to as programmed anisotropy.[18] This principle has been adopted to alter the shape-induced magnetic anisotropy of superparamagnetic helical swimmers by setting their magnetic easy axis, significantly improving their locomotion characteristics.[15] While the helical actuator shape is favorable the locomotion, it provides limited loading capacity for surface coatings. Swimming microrobots with increased surface area are highly desirable for advanced biomedical applications.

In this work, the concept of programmed anisotropy is combined with two-photon polymerization (TPP) of a superparamagnetic polymer composite to enable the fabrication of a new class of magnetic twist-type micro actuators with imprinted, shape-independent magnetic properties. In comparison to helical microswimmers, the proposed devices possess a significantly increased surface area while providing comparable feature sizes, actuation, and locomotion characteristics. In order to demonstrate twist-type microswimmers as a wirelessly actuated platform for biomedical applications, a versatile functionalization strategy is addressed to exploit the actuator's increased surface area. Direct and indirect surface functionalization based

C. Peters, M. Müller, Prof. C. Hierold
Micro and Nanosystems, ETH Zurich
Tannenstrasse 3, 8092, Zurich, Switzerland
E-mail: chpeters@ethz.ch
Dr. O. Ergeneman, P. D. W. García,
Dr. S. Pané, Prof. B. J. Nelson
Institute of Robotics and Intelligent Systems, ETH Zurich
Tannenstrasse 3, 8092, Zurich, Switzerland
E-mail: vidalp@ethz.ch

DOI: 10.1002/adfm.201400596

on human immunoglobulin (HIgG), fluorescein isothiocyanate (FITC), and FITC-tagged goat antihuman immunoglobulin (Ga HIgG FITC) are employed and successful surface modification is demonstrated based on fluorescence assays.

2. Twist-Type Actuators with Programmed Magnetic Anisotropy

2.1. Programmed Anisotropy in SU-8 Based Composite Films

The twist-type actuators are fabricated from a superparamagnetic polymer composite (SPMPC) consisting of superparamagnetic magnetite nanoparticles (Fe_3O_4, 11 nm particle diameter, measured by transmission electron microscopy (TEM)), dispersed in commercial SU-8 negative tone photoresist.[19] During conventional composite processing for single and TPP, i.e. spin-coating, baking and exposure, the iron oxide nanoparticles are randomly distributed within both the composite solution as well as the dried and eventually cross-linked polymer matrix. The magnetic properties of these films and, subsequently, the magnetic properties of the fabricated devices are governed by geometric effects (shape anisotropy). If a magnetic field is applied during composite soft baking, the external field magnetizes the single-domain superparamagnetic iron oxide particles and aligns their magnetic moment parallel to the external field. Attractive forces between the individual particles induce a directed self-organization, leading to the formation of particle chains, also oriented in the direction of the external field. The composite solvent γ-butyrolactone (GBL) evaporates from the film during the soft-bake and the particles become locked in the dried polymer film, preserving their alignment when the external field is removed. This is different from the approach presented by Kim et al., where particle alignment can only be preserved once the liquid polymer is cross-linked. However, in both cases, the formation of particle lines can be observed using (transmission light) microscopy.[15] The direction in which the particles are aligned represents the preferred direction of magnetization and is referred to as the magnetic easy axis. As the particles remain locked during lithography and subsequent processing, both particle alignment and directionality of the particle anisotropy remain unchanged and are imprinted into the fabricated device. Combining this approach with TPP instead of conventional lithography enables the fabrication of truly three-dimensional microactuators with complex shapes and shape-independent magnetic properties.

2.2. Programmed Anisotropy in Twist-Type Actuators

Three different types of twist-type actuators are investigated in this work: helical actuators, single twist-type actuators and double twist-type actuators. The cross-section of these actuators is as follows: helical actuators are characterized by a circular cross-section with eccentric location, single twist-type actuators are characterized by a point-symmetric bar-shaped cross-section, and double twist-type actuators are characterized by a point-symmetric cross-shaped cross section. The three-dimensional actuator shape evolves by a twisted extrusion of the cross section along the rotational axis (which is perpendicular to the cross-section and penetrates the center point). Front and side views of the three different actuator designs are illustrated in **Figure 1**a. For a better assessment, technical drawings and a more detailed explanation can be found in the Supporting Information Figure S1. For each actuator type, five different actuator designs with actuator pitch angles θ ranging from 30° to 60° were designed. Herein θ is referred to as the angle between rotational axis (length axis) and the inclination of the filament pitch (see Supporting Information Figure S1). In order to compare the performance of different actuator designs, all actuators are characterized by an outer diameter of approximately 9 µm and a length of 60 µm. The actuator's geometrical properties are derived from the mechanical models and summarized in **Table 1**. In comparison to helical actuators, the surface area and, thus, the load capacity of single and double twist-type actuators increases by a factor of more than 1.5 and 3, respectively. While all actuator types possess comparable feature sizes, the increase in surface area—and subsequently the increase in load capacity—evolves only from the different actuator shapes.

The proposed process flow for the fabrication of helical, single and double twist-type actuators with engineered magnetic properties is illustrated in Figure 1b. After composite spin-coating (top left) particles are randomly distributed as indicated in the zoomed view. Particle alignment within the non-cross-linked polymer film is established by applying a homogeneous magnetic field of 30 mT during soft bake as indicated in Figure 1b top right. The magnetic field is oriented in-plane as indicated by the arrow. The related transition in particle alignment as well as the newly established easy axis are illustrated in the zoom views. The writing patterns utilized for TPP are oriented such that the rotation axis of the fabricated devices is perpendicular to the previously applied magnetic field, implementing a magnetic easy axis perpendicular to the rotational axis of the fabricated devices. After TPP and post exposure bake, unexposed composite is removed and the fabricated devices remain on the wafer surface (Figure 1b, center). For comparison, shape-anisotropic twist-type actuators are fabricated by applying TPP to SPMPC films with randomly aligned particles. A more detailed explanation of the composite processing is laid out in the experimental section of this work. Below, twist-type actuators with manipulated magnetic easy axis will be referred to as manipulated twist-type actuators while shape-anisotropic twist-type actuators will be referred to as reference twist-type actuators. Electron microscopy pictographs of the different actuators investigated in this work are depicted in Figure 1c–e. Figure 1c shows an overview of the fifteen different actuators. Figure 1d and e show zoomed top-views of a single twist-type actuator with a pitch of 30° and a double twist-type actuator with a pitch angle of 30°, respectively. In contrast to previous fabrication approaches, the actuator surface is not smooth, but possesses a step-like surface profile.[15] This characteristic emerges as the TPP patterns have been derived from a CAD file rather than a continuous trajectory.

2.3. Twist-Type Actuators in Liquid Environments

The magnetic anisotropy in twist-type actuators is investigated by subjecting the fabricated devices to stationary and rotating

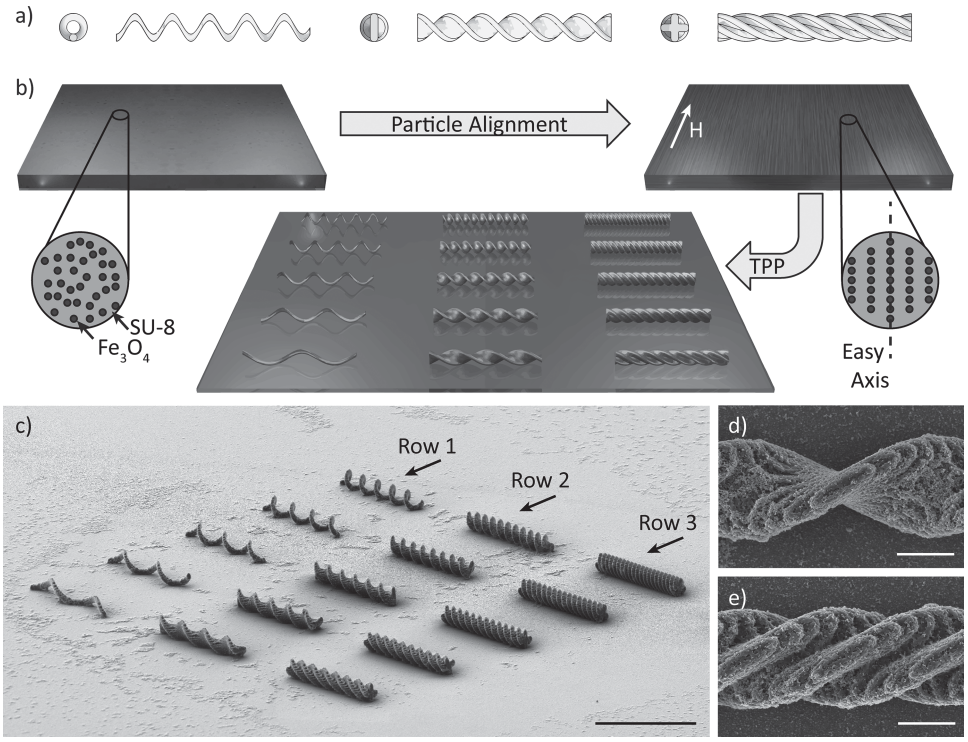

Figure 1. a) Conceptual drawing of swimming microrobots investigated in this work displayed in front and side view: left: helical swimming microrobots; center: single twist-type actuators, right: double twist-type actuators; b) Fabrication of swimming microrobots with engineered magnetic properties consisting of spin coating (top left), particle alignment (top right) and two-photon polymerization (TPP, center), particle distribution is indicated in the zoom views, magnetic field direction and direction of the easy axis are indicated by the arrow/dashed lines, respectively; c) Tilted electron microscopy image of the fabricated helical actuators (Row 1), single twist-type actuators (Row 2) and double twist-type actuators (Row 3), scale bar 50 µm; d,e) Top view of a single and double twist-type actuator with a pitch of 30°, respectively, scale bars: 5 µm.

Table 1. Geometrical properties of twist-type actuators investigated in this work; for definition of the device pitch angle, please refer to Supporting Information S1; the comparison of geometrical properties reveals that single and double twist-type actuators possess an increased surface area A and thus an increased load capacity in comparison to helical actuators.

Actuator Type	Device pitch angle θ [°]	Number of Turns	A [µm^2]
Helical	30.0	1.7	499.6
	37.5	2.3	524.8
	45.0	3.0	562.1
	52.5	3.9	618.9
	60.0	5.2	710.3
Single Twist	30.0	1.7	1343.4
	37.5	2.3	1397.8
	45.0	3.0	1479.0
	52.5	3.9	1603.8
	60.0	5.2	1806.6
Double Twist	30.0	1.7	2091.8
	37.5	2.3	2197.0
	45.0	3.0	2354.1
	52.5	3.9	2594.8
	60.0	5.2	2984.1

magnetic fields. The fabricated devices are immersed in DI-water, placed in the center of a three axis Helmholtz manipulator, and released from their substrate. Details about the Helmholtz manipulator and the release technique are described in the Supporting Information. When the released devices are subjected to a homogeneous magnetic field, the devices align such that their magnetic easy axis aligns parallel to the external field. The alignment of reference and manipulated twist-type actuators has been investigated by applying a homogeneous magnetic field of 5 mT and is shown in **Figure 2**a for single twist-type actuators with a device pitch angle of 45°. Shape-anisotropic effects are governed by demagnetization fields, which are the weakest along the longest dimension of a soft magnetic body. In reference twist-type actuators, the longest geometrical expansion occurs along the rotational axis, implying the presence of a shape-anisotropic magnetic easy axis along the rotational axis itself. However, the actuator's twisted shape tilts the magnetic easy axis slightly away from the rotational axis (Figure 2a top). The alignment of manipulated twist-type actuators is governed by the programmed anisotropy, explaining the perpendicular alignment of manipulated twist-type actuators (Figure 2a bottom).

The orientation of the magnetic easy axis has significant implications on the actuation of the superparamagnetic devices, i.e. the magnetic torque normal is oriented perpendicular to the plane held by the magnetic easy axis of the device and the

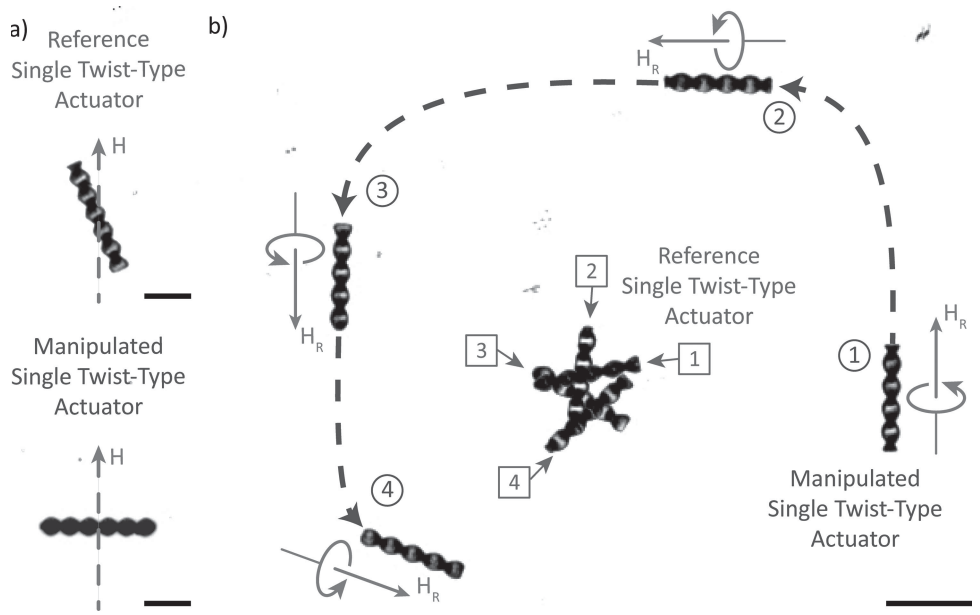

Figure 2. a) Alignment of reference and manipulated single twist-type actuators subjected to a homogeneous field of H = 5 mT as indicated by the dashed arrows, alignment of reference devices is governed by shape-anisotropic effects, alignment of manipulated devices is governed by the programmed anisotropy, all scale bars are 20 μm; b) Image sequence of single twist-type actuators subjected to rotational fields of H_R = 5 mT, rotational field normal indicated by the solid arrow: While manipulated actuators perform cork screw-propulsion, reference devices are only rotated about their center of gravity; scale bar is 50 μm; a similar video sequence can be found in the Supporting Information Video V1.

external magnetic field.[20] Hence, manipulated twist-type actuators are capable of performing cork-screw propulsion, whereas reference twist-type actuators are being rotated about their center of gravity. An image sequence of this behavior is illustrated in Figure 2b. These observations underline the importance of the programmed anisotropy as an enabling technology for superparamagnetic sensors and actuators and highlight the necessity of particle self-organization in order to enable desirable actuation and locomotion strategies. In particular, wobble-free locomotion at low excitation frequencies as well as out-of-plane locomotion, i.e. overcoming gravity, are enabled (reference video of a 45° single twist-type actuator can be found in the Supporting Information Video V1). The origin of wobbling and its limitations on device actuation are characterized elsewhere.[16,21]

Figure 3 shows a quantitative evaluation of both forward velocity and drift velocity as a function of excitation frequency for single and double twist-type actuators as well as for helical actuators. Herein, forward velocity is defined as the velocity measured along the direction of the rotational field normal while the drift velocity is defined as the velocity perpendicular to it. For a better assessment, drift velocities are displayed with a negative sign. The drift itself results from a "rolling" of the device on the surface.[21] For all experiments a rotational magnetic field with a strength of 5 mT is applied. Helical actuators with pitch angles of 37.5°, 45°, 52.5°, and 60° possess a linear relation between forward velocity and excitation frequency until they reach their maximum forward velocity. The frequency at which the maximum forward velocity is achieved is known as step-out frequency.[2] Excitation frequencies in excess of the step-out frequency lead to a loss of synchronicity between excitation frequency and rotational frequency of the actuator and subsequently to a decrease in forward velocity. For helical actuators with a pitch angle of 30°, drift velocities increase significantly and recover again for excitation frequencies above 10 Hz. This observation is attributed to the fact that the swimmers possess less than two turns (see Table 1) and are not fully stable for excitation frequencies below 10 Hz. Accordingly, the relation between forward velocity and excitation frequency is not linear. For single twist-type actuators, similar behavior is observed, i.e. non-linear forward velocity vs. excitation frequency relation for devices with a pitch angle of 30° and linear forward velocity vs. excitation frequency relation for all other devices below step-out. It has to be noted that the step-out frequency for single twist-type actuators with a pitch of 60° was not observed and must exceed 20 Hz. Single twist-type actuators possess an increased drift velocity in comparison to helical actuators, but forward velocity is still dominant. For double twist-type actuators, drift velocity exceeds forward velocity and surface drift becomes more efficient than cork-screw propulsion. Reasonable forward velocities were observed for actuators with a pitch of 30° and 37.5°. For better assessment, maximum forward velocities as well as the related step-out frequencies are displayed in **Table 2**. Single twist-type actuators and helical actuators possess comparable forward velocities of over one body length per second. The increased load capacity of single twist-type actuators does not compromise the device actuation itself. For double twist-type actuators with a pitch of 30° and 37.5°, the forward velocity is decreased by less than 50%. The increase in surface area of more than 300% outweighs the decreased forward velocity and makes these actuators suitable candidates when high loading capacities are required.

The decrease in forward velocity and the increase in drift velocity moving from helical actuators to double twist-type

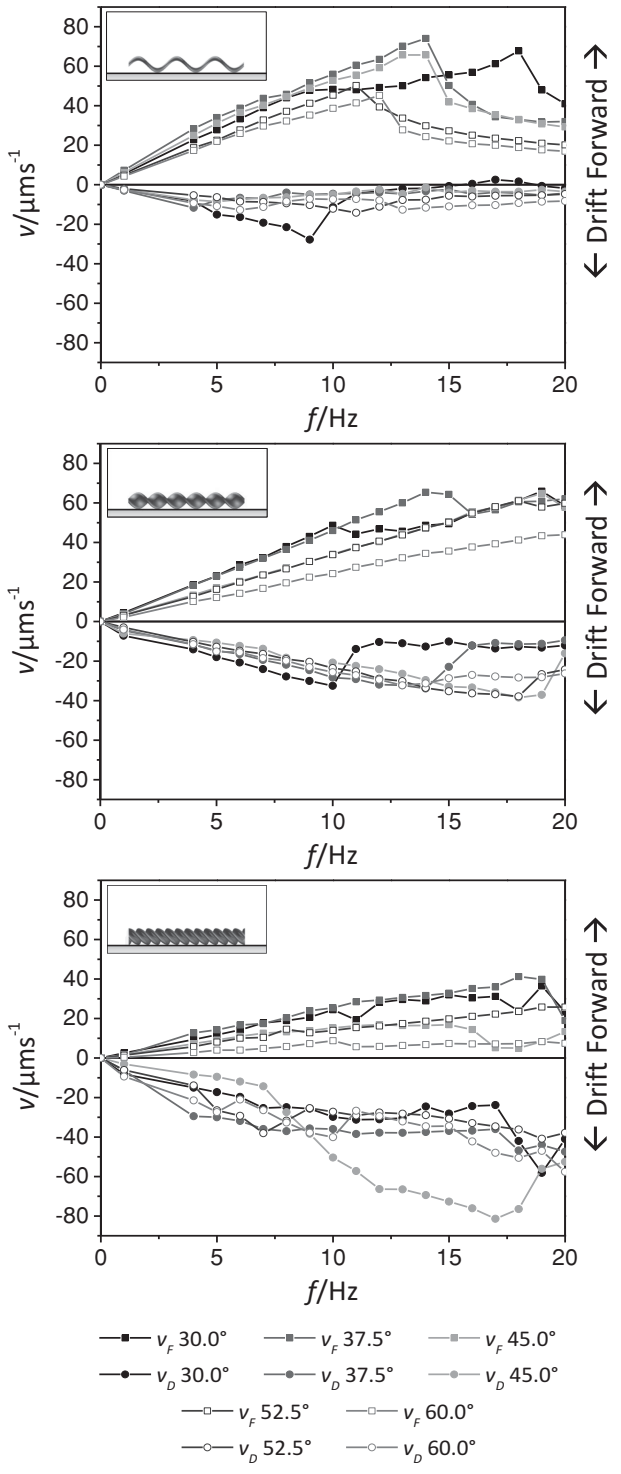

Figure 3. Forward velocity v_F and drift velocity v_D of twist-type actuators with different device pitch angles as indicated in the legend; Top: Helical actuators, middle: single twist-type actuators, bottom: double twist-type actuators; For all experiments, a rotational magnetic field of $H_R = 5$ mT has been applied.

actuators can be explained with a simple, but instructive analogy. An ideal, slender helical structure can generate a maximum forward thrust without drifting, whereas a cylinder cannot generate forward thrust and can only drift sideways. Helical actuators discussed in this work can be approximated by a slender helix, i.e. they possess a high forward velocities and small drift velocities. Single twist-type actuators possess an increased cross-sectional area and the structure appears as an intermediate between slender helix and cylinder: Forward velocities are still high but drift velocities increase. Double twist-type actuators possess the highest cross-sectional area and the approximation of a cylinder becomes more reasonable: Drift velocities become more pronounced and surpass forward velocities.

Table 2. Comparison of maximum forward velocities and step-out frequencies of selected helical, single and double twist-type actuators, the underlying data is presented in Figure 3, blank fields indicate that no (reasonable) step-out frequency was observed.

Pitch Angle	Helical Actuator	Single Twist Actuator	Double Twist Actuator
30°	67.8 µm s^{-1} / 18 Hz	66.0 µm s^{-1} / 19 Hz	36.5 µm s^{-1} / 19 Hz
37.5°	74.1 µm s^{-1} / 14 Hz	65.4 µm s^{-1} / 14 Hz	41.3 µm s^{-1} / 18 Hz
45°	65.7 µm s^{-1} / 13 Hz	64.8 µm s^{-1} / 19 Hz	—
52.7°	50.2 µm s^{-1} / 11 Hz	61.2 µm s^{-1} / 18 Hz	—
60°	45.2 µm s^{-1}/12 Hz	—	—

3. Surface Functionalization

The actuator's increased load capacity is exploited by a facile functionalization strategy based on glycine grafting and subsequent Human Immunoglobulin immobilization. This approach allows for a specific attachment of bio-molecules and drugs on the actuator surface, providing for a versatile microrobotic platform for biomedical applications. For surface functionalization, samples are cleaned with IsoPropyl Alcohol (IPA) and rinsed with DI-water, then treated with NaOH and HCl leading to a cleavage of parts of the epoxy groups and subsequent protonation of the formed carboxylates (**Figure 4**a, step 1). A posterior incubation in glycine induces formation of secondary amines by reaction with the remaining epoxy groups, and in the case of available hydroxyl groups, glycine amines are bonded through hydrogen bonds and electrostatic attraction (Figure 4a, step 2).[22] A successive treatment with a 1-ethyl-3-(3-dimethylaminopropyl) carbodiimide:*N*-hydroxysuccinimide (EDC:NHS) solution is conducted. First, EDC reacts with the carboxylic groups of glycine leading to an unstable O-acylisourea active ester. Then NHS displaces EDC by nucleophilic attack creating a stable amine-reactive NHS Ester (Figure 4a, steps 3 and 4). Consequently, the surface is ready for conjugation to primary amines, for instance, the ones present in immunoglobulin. This procedure enables the immobilization of HIgG on SU-8 substrates.

The success of the surface functionalization is evaluated by fluorescence assays. Both, direct and indirect tagging of the surface were performed. While direct tagging may be utilized to evaluate the functionalization procedure, indirect tagging provides for a generic functionalization platform that can be utilized for various biomedical applications as denoted above. Direct tagging is performed by incubating the prepared

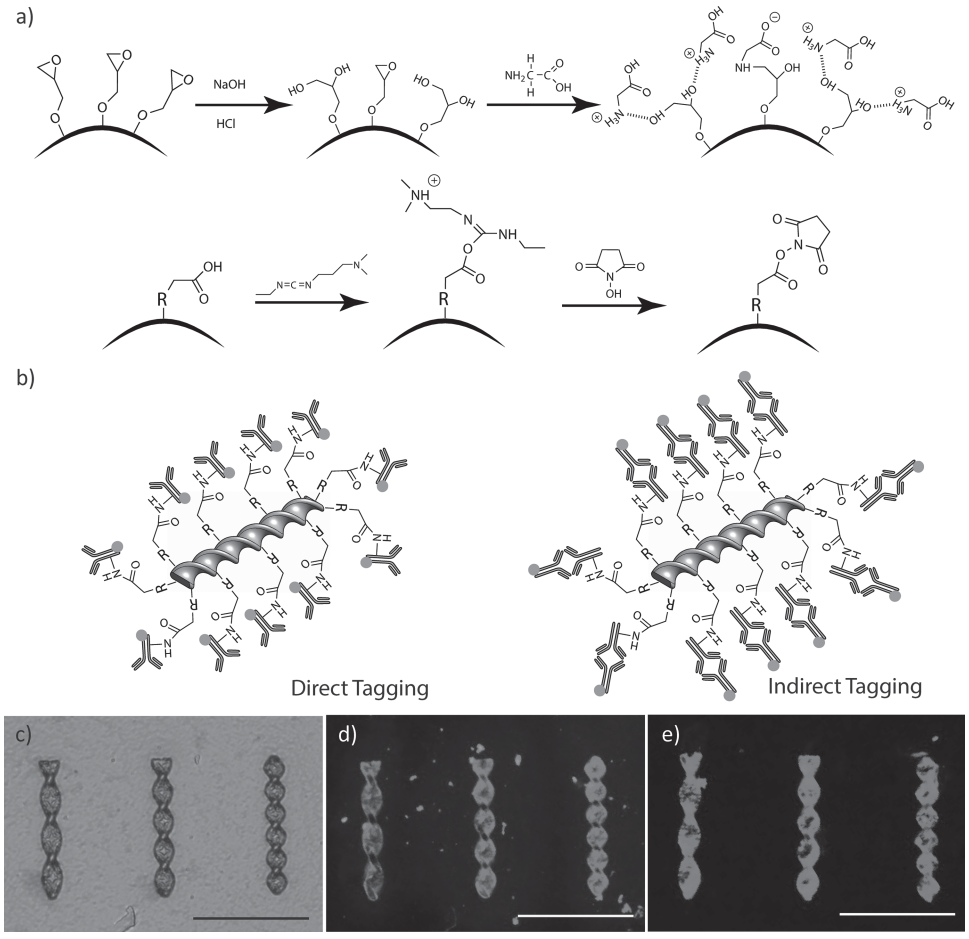

Figure 4. a) Schematic process of the generic surface modification; b) Functionalization strategy for direct and indirect tagging; c) to e) Microscopy image of single twist-type actuators with different pitch angles (37.5° to 52.5°), c) Light microscopy image before functionalization, d) Fluorescence microscopy image of directly tagged actuators, e) Fluorescence microscopy image of indirectly directly tagged actuators; all scale bars are 50 μm.

samples in FITC tagged HIgG solution. Indirect tagging is performed by incubating HIgG treated samples in Ga HIgG FITC tagged solution. A more detailed overview about these immunoassays can be found in the experimental section of this work.

In order to exclude particle related effects during surface functionalization, protein immobilization and fluorescence tagging were first performed using pristine SU-8 samples. A set of five differently treated samples was prepared. Sample 1 was cleaned with IPA and DI water and served as a control to discard SU-8 auto-fluorescence at the investigated wavelength. Sample 2 was cleaned and treated with FITC tagged HIgG, and sample 3 was cleaned and treated with non-tagged HIgG and subsequently treated with fluorescence tagged Ga HIgG. Samples 2 and 3 are used to exclude non-specific protein absorption onto SU-8. Samples 4 and 5 were cleaned, pretreated, activated and either treated with fluorescence tagged HIgG or with HIgG solution and subsequently fluorescence tagged Ga HIgG. Fluorescence analysis was carried out using an inverted fluorescent microscope. The control sample exhibited no auto fluorescence at 510–550 nm emission and 460–495 nm excitation wavelength, omitting the necessity of fluorescence subtraction. Samples 2 and 3 did not show a fluorescence response, revealing that non-specific protein absorption does not occur. In contrast, samples 4 and 5 show a sufficient concentration of immobilized fluorescence tags, confirming the proposed functionalization approach. The related fluorescence images are illustrated in the Supporting Information Figure S2.

After verifying the functionalization protocol, fabricated and characterized twist-type actuators were treated accordingly. Two sets of samples were investigated. Set one was pretreated, activated and directly tagged, and set two was pretreated, activated and indirectly tagged. The related schematics and microscope images are depicted in Figure 4b and c. All samples were transferred to a 5-DOF magnetic manipulation setup equipped with a fluorescence camera setup as described above. Further details about the 5-DOF magnetic setup and the device release can be found in the Supporting Information. Directly and indirectly tagged samples show a strong fluorescence response as depicted in Figure 4d and e. A video sequence showing the locomotion of an indirectly tagged single twist-type actuator with a device pitch angle of 45° can be found in the Supporting Information Video V1. This video eventually connects the individual aspects of this work: Material properties and fabrication strategies are engineered

to enable novel actuators with superior properties while the applied surface functionalization exploits the novel actuator shape, demonstrating the full potential of the twist-type actuator platform with a generic functionalization strategy for various biomedical applications.

4. Discussion

The twist-type actuators possess a feature size which is more than one order of magnitude smaller than any other twist-type actuator demonstrated to date,[23] enabling advanced biomedical applications at locations that are not reachable for those devices. In comparison to helical microswimmers, the single and double twist-type actuators possess a significant increase in surface area, enabling increased load capacity for biomedical applications. The actuators are characterized by a lower maximum velocity (just over one bodylength/second) compared to swimming microrobots fabricated by TPP of pristine SU-8 photoresist and subsequent evaporation of magnetic material (10 to 15 body lengths/second) and those fabricated by template assisted electrodeposition (3 body lengths/second).[24] Similar performance ratios are observed in comparison to artificial magnetotactic bacteria propelled by catalytic bubble ejection where forward velocities between 6 and 18 body lengths/second are observed.[25] The maximum forward velocity of the presented twist-type actuators can be increased by increasing the step-out frequency. This can be achieved by increasing the strength of the external magnetic field and/or by increasing the swimmer's magnetization, which is proportional to the particle load. The increase in particle load can be achieved by overcoming the particle-induced absorption by introducing novel photo initiators to form the SU-8 polymer composite network in a more efficient manner.[26] The velocity vs. input frequency relation is dependent on the pitch angle. Hence, utilizing twist-type actuators with different pitch angles, input frequency regulated swarm control can be performed.[2]

5. Conclusion

The combination of TPP and programmed magnetic anisotropy enables the fabrication of complex three-dimensional devices with shape-independent magnetic properties. Based on this approach superparamagnetic sensors and actuators with tailored magnetic properties can be realized as demonstrated by the twist-type microactuators. In particular, we demonstrated swimming microrobots that have neither been fabricated from a superparamagnetic material itself nor from any other material at this scale. Furthermore, we demonstrated efficient swimming performance by cork-screw propulsion. The swimming microrobots were capable of performing wobble-free rotation and out-of-plane swimming. The actuator's increased surface area was exploited by a versatile functionalization strategy. Fluorescence assays showed that twist-type actuators can serve as a platform for many biomedical applications such as on-demand, targeted drug delivery and remote sensing.

6. Experimental Section

Actuator Design and Fabrication: Twist-type actuators have been designed using a 3D CAD tool (Autodesk Inventor). The design files were converted into STereo Lithography (STL) language and translated into General Writing Language (GWL) utilized for the NanoScribe Professional Photonics TPP tool. The SPMPC used in this work is obtained by dispersing a superparamagnetic magnetite FerroFluid (FF) into commercially available SU-8 negative tone photoresist (micro resist technology GmbH, Berlin/Germany). More details about the FF are given in the Supporting Information. The FF is dispersed in commercial SU-8 photoresist using a Hauschild DAC 150 planetary mixer for 10 miutes and sonicated in a Sonics & Materials Inc. Vibracell VCX 600 ultrasound system for 20 min. The particle content is adjusted to achieve a final concentration of 2%vol with respect to the solid SU-8 content. The SPMPC is spin-coated on transparent 30 mm glass wafers with a speed of 1000 rpm for 20 s. For the fabrication of manipulated ABF, the spin coated wafer is transferred to a custom-made Helmholtz coil setup equipped with a hotplate. Soft bake is carried out for 60 min at 75 °C in the presence of a homogenous magnetic field of 30 mT. The samples are then transferred to a NanoScribe Photonics Professional Tool (NanoScribe GmbH, Karlsruhe/Germany). The samples are aligned such that their easy axis is oriented in perpendicular to the rotational axis of the to-be fabricated devices. TPP is carried out using an oil immersion microscope with a magnification of 100×, NA 1.4 at a writing speed of 50 µm/s and a laser power of 1.4 mW. The exposed samples are transferred back to the Helmholtz coil setup and post exposure bake is carried out at 95 °C for 4 min in order to cross-link the polymer matrix. During post exposure bake, a homogeneous magnetic field of 30 mT is applied in order to maintain the particle alignment. Non cross-linked resist is removed by developing the samples in mr-Dev 600 developer (micro resist technology GmbH, Berlin/Germany) for 4 min and isopropyl alcohol (IPA) for 1 min. Samples are then dried in air. Shape-anisotropic reference devices are fabricated in the same manner except that no particle alignment is performed.

Surface Functionalization: IPA, sodium hydroxide (NaOH), hydrogen chloride (HCl), glycine, 1-ethyl-3-(3-dimethylaminopropyl) carbodiimide (EDC), *N*-hydroxysuccinimide (NHS), bovine serum albumin (BSA), polysorbate 20 (Tween 20), human immunoglobulin (HIgG), fluorescein isothiocyanate (FITC), and goat antihuman immunoglobulin FITC (Ga HIgG FITC) were purchased from Sigma Aldrich (Switzerland). All reagents were of analytical quality or better and used as received. The following stock solutions were prepared: NaOH in DI water (0.1 M), HCl in DI water (1 M); glycine in DI water (5 mM); EDC: NHS in DI water (0.2 M : 0.1 M); PBS + Tween 20 + BSA (0.05%vol + 1 mg/mL, solution referred to as PBTSB); HIgG in PBS (0.05 mg/mL); Ga HIgG + BSA in DI water (0.05 mg/mL + 2 mg/mL); and Ga HIgG FITC in PBS (0.01 mg/mL). Preparation for both direct and indirect fluorescence stats with the following common steps: SU-8 Samples are rinsed with DI-water and IPA, dried and immersed in NaOH solution (5 mL) for 10 min, in HCl solution (5 mL) for 10 min and glycine solution (5 mL) for another 2 h. After incubation, samples are dried and the sample surface is subsequently covered with EDC:NHS solution (1 mL) incubated for one hour and dried. Samples used for direct fluorescence assays are covered with HIgG FITC solution (1 mL) and incubated over night at 4 °C. The incubated samples are rinsed three times with PBTSB solution. Samples used for indirect fluorescence assays are covered with HIgG solution (1 mL) and incubated over night at 4 °C and rinsed three times with PBSTB solution. The samples are covered with Ga HIgG solution (1 mL) and incubated for 2 h and again rinsed three times with PBTSB solution.

Supporting Information

Supporting Information is available from the Wiley Online Library or from the author.

Acknowledgements

The authors would like to thank Mahmut Selman Sakar (ETH Zurich) for his contributions to fluorescence visualization. Furthermore, we would like to thank the FIRST-CLA cleanroom staff for their support throughout the project. This work has been carried out in the framework of SelfSys, scientifically evaluated by SNSF as well as financed by the Swiss Confederation and funded by Nano-Tera.ch as well as the Swiss National Science Foundation, grant no 200021_130069/1.

Received: February 20, 2014
Revised: March 25, 2014
Published online: May 23, 2014

[1] B. J. Nelson, I. K. Kaliakatsos, J. J. Abbott, *Annu. Rev. Biomed. Engineering* **2010**, *12*, 55.
[2] K. E. Peyer, L. Zhang, B. J. Nelson, *Nanoscale* **2013**, *5*, 1259.
[3] E. B. Steager, M. Selman Sakar, C. Magee, M. Kennedy, A. Cowley, V. Kumar, *Int. J. Robotics Res.* **2013**, *32*, 346.
[4] a) S. Tottori, L. Zhang, F. Qiu, K. K. Krawczyk, A. Franco-Obregón, B. J. Nelson, *Adv. Mater.* **2012**, *24*, 709; b) S. Floyd, C. Pawashe, M. Sitti, *Robotics, IEEE Trans.* **2009**, *25*, 1332.
[5] a) B. H. McNaughton, J. N. Anker, R. Kopelman, *J. Magn. Magn. Mater.* **2005**, *293*, 696; b) O. Ergeneman, G. Dogangil, M. P. Kummer, J. J. Abbott, M. K. Nazeeruddin, B. J. Nelson, *IEEE Sens. J.* **2008**, *8*, 29.
[6] O. Ergeneman, J. J. Abbott, G. Dogangil, B. J. Nelson, presented at the 2nd IEEE RAS & EMBS International Conference Biomedical Robotics and Biomechatronics, 19–22 Oct. 2008.
[7] K. E. Peyer, S. Tottori, F. Qiu, L. Zhang, B. J. Nelson, *Chem. Eur. J.* **2013**, *19*, 28.
[8] a) K. L. Prime, G. M. Whitesides, *J. Am. Chem. Soc.* **1993**, *115*, 10714; b) G. L. Kenausis, J. Vörös, D. L. Elbert, N. Huang, R. Hofer, L. Ruiz-Taylor, M. Textor, J. A. Hubbell, N. D. Spencer, *J. Phys. Chem. B* **2000**, *104*, 3298; c) R. G. Chapman, E. Ostuni, S. Takayama, R. E. Holmlin, L. Yan, G. M. Whitesides, *J. Am. Chem. Soc.* **2000**, *122*, 8303.
[9] J. V. Frangioni, *J. Clinical Oncol.* **2008**, *26*, 4012.
[10] S. Fusco, G. Chatzipirpiridis, K. M. Sivaraman, O. Ergeneman, B. J. Nelson, S. Pané, *Adv. Healthcare Mater.* **2013**, *2*, 1037.
[11] a) F. Sato, M. Jojo, H. Matsuki, T. Sato, M. Sendoh, K. Ishiyama, K. I. Arai, *IEEE Trans. Magnetics* **2002**, *38*, 3362; b) M. Sendoh, K. Ishiyama, K. I. Arai, M. Jojo, F. Sato, H. Matsuki, *IEEE Trans. Magnetics* **2002**, *38*, 3359; c) R. Hergt, W. Andrä, in *Magnetism in Medicine*Wiley-VCH Verlag, Germany **2007**, p. 550.
[12] a) C. Brazel, *Pharm. Res.* **2009**, *26*, 644; b) N. S. Satarkar, S. A. Meenach, K. W. Anderson, J. Z. Hilt, *AIChE Journal* **2011**, *57*, 852.
[13] L. Zhang, K. E. Peyer, B. J. Nelson, *Lab Chip* **2010**, *10*, 2203.
[14] a) H. C. Berg, R. A. Anderson, *Nature* **1973**, *245*, 380; b) E. M. Purcell, *Am. J. Phys.* **1977**, *45*, 3.
[15] C. Peters, O. Ergeneman, B. J. Nelson, C. Hierold, presented at the IEEE 26th International Conference on Micro Electro Mechanical Systems, 20–24 Jan. 2013, DOI: 10.1109/MEMSYS.2013.6474304
[16] M. Suter, L. Zhang, E. Siringil, C. Peters, T. Luehmann, O. Ergeneman, K. Peyer, B. Nelson, C. Hierold, *Biomed. Microdevices* **2013**, 1.
[17] K. Peyer, E. Siringil, L. Zhang, M. Suter, B. Nelson, in *Biomimetic and Biohybrid Systems*, Vol. *8064* (Eds: N. Lepora, A. Mura, H. Krapp, P. M. J. Verschure, T. Prescott), Springer, Berlin/Heidelberg, **2013**, p. 216.
[18] J. Kim, S. E. Chung, S.-E. Choi, H. Lee, J. Kim, S. Kwon, *Nat. Mater.* **2011**, *10*, 747.
[19] M. Suter, O. Ergeneman, J. Zürcher, C. Moitzi, S. Pané, T. Rudin, S. E. Pratsinis, B. J. Nelson, C. Hierold, *Sens. Actuat. B* **2011**, *156*, 433.
[20] J. J. Abbott, O. Ergeneman, M. P. Kummer, A. M. Hirt, B. J. Nelson, *IEEE Trans. Robotics* **2007**, *23*, 1247.
[21] K. E. Peyer, Z. Li, B. E. Kratochvil, B. J. Nelson, presented at the IEEE International Conference on Robotics and Automation (ICRA), 3–7 May 2010.
[22] A. Deepu, V. V. R. Sai, S. Mukherji, *J. Mater. Sci. Mater. Med.* **2009**, *20*, 25.
[23] K. Kobayashi, K. Ikuta, presented at the IEEE 22nd International Conference on Micro Electro Mechanical Systems, 25–29 Jan. 2009.
[24] a) L. Z. S. Tottori, F. Qiu, K. Krawczyk, A. Franco-Obregón, B. J. Nelson, *Adv. Mater.* **2012**, *24*, 811; b) M. A. Zeeshan, R. Grisch, E. Pellicer, K. M. Sivaraman, K. E. Peyer, J. Sort, B. Özkale, M. S. Sakar, B. J. Nelson, S. Pané, *Small* **2013**, *10*, 1284.
[25] a) G. Zhao, M. Pumera, *Langmuir* **2012**, *29*, 7411; b) G. Zhao, S. Sanchez, O. G. Schmidt, M. Pumera, *Chemical Commun.* **2012**, *48*, 10090.
[26] C. Peters, O. Ergeneman, B. J. Nelson, C. Hierold, Proc. Int. Conf. on Solid-State Sensors, Actuators and Microsystems Conference (TRANSDUCERS), Barcelona,2013, pp. 2676, DOI: 10.1109/Transducers.2013.6627357.